Principles of PET/MR Imaging

Jonathan A. Disselhorst[1], Ilja Bezrukov[1,2], Armin Kolb[1], Christoph Parl[1], and Bernd J. Pichler[1]

[1]*Werner Siemens Imaging Center, Department of Preclinical Imaging and Radiopharmacy, Eberhard Karls University of Tübingen, Tübingen, Germany; and* [2]*Max-Planck-Institute for Intelligent Systems, Tübingen, Germany*

Hybrid PET/MR systems have rapidly progressed from the prototype stage to systems that are increasingly being used in the clinics. This review provides an overview of developments in hybrid PET/MR systems and summarizes the current state of the art in PET/MR instrumentation, correction techniques, and data analysis. The strong magnetic field requires considerable changes in the manner by which PET images are acquired and has led, among others, to the development of new PET detectors, such as silicon photomultipliers. During more than a decade of active PET/MR development, several system designs have been described. The technical background of combined PET/MR systems is explained and related challenges are discussed. The necessity for PET attenuation correction required new methods based on MR data. Therefore, an overview of recent developments in this field is provided. Furthermore, MR-based motion correction techniques for PET are discussed, as integrated PET/MR systems provide a platform for measuring motion with high temporal resolution without additional instrumentation. The MR component in PET/MR systems can provide functional information about disease processes or brain function alongside anatomic images. Against this background, we point out new opportunities for data analysis in this new field of multimodal molecular imaging.

Key Words: positron emission tomography; magnetic resonance imaging; multimodal imaging; instrumentation

J Nucl Med 2014; 55:2S–10S
DOI: 10.2967/jnumed.113.129098

With nuclear imaging, biologic processes can be visualized and measured at the molecular level. There is ever-increasing interest in pushing the limits of multimodal molecular/anatomic imaging, and there is now the new hybrid of PET/MR. The combination of these 2 modalities into a single machine reduces registration errors and, for simultaneous scanning, can reduce the imaging time. Although the resolution of modern PET scanners is reasonably high, at approximately 4–5 mm full width at half maximum at the center of the field of view (FOV) for clinical systems, additional anatomic information is beneficial, especially when tracers with a high specificity for a certain target are used. For this purpose, combined PET/CT was introduced more than 10 y ago (*1*). However, MR can provide anatomic information with much higher soft-tissue contrast without the additional radiation dose from CT. Another major advantage of MR is that it can provide functional information in addition to anatomic data. However, the sensitivity of PET is much higher than that of MR ($\sim 10^{-12}$ mol/L for PET vs. $\sim 10^{-5}$ mol/L for MR); thus, PET remains an essential component of molecular imaging. Nevertheless, combining the functional data obtained with both modalities can provide complementary information about, for example, disease processes and the function of the brain as well as aid in reaching a diagnosis. MR can provide the following types of functional information, among others: perfusion, diffusion, and spectroscopy to reveal metabolites. Additional advantages of PET/MR are the potential for motion correction, as well as reconstruction driven by anatomic information (*2,3*).

Another advantage of PET/MR, which was a driving force in the initial development of combined PET/MR, is the reduction of the positron range in a magnetic field. The distance positrons travel before annihilation, especially for higher field strengths, is reduced in the direction orthogonal to the magnetic field, leading to in-plane improvement in the resolution proportional to the field strength (*4*).

The first attempts to combine MR and PET were performed with images acquired on separate machines; the images were subsequently coregistered (*5*). This works well in the brain but is more cumbersome in organs that have more motion. The use of a single imaging device to acquire both modalities makes image registration more straightforward and enables whole-body imaging with multiple modalities. Early PET/MR devices were described and designed (*4,6*) even before the introduction of PET/CT (*1*). Hybrid PET/CT scanners have greatly improved the usefulness of PET by enabling accurate anatomic localization of pathologies and have completely replaced stand-alone PET devices. In the meantime, hybrid PET/MR has remained a field of active research.

Despite more than 2 decades of ongoing research and interest in combined PET/MR, only a small number of systems are currently commercially available (Table 1). Several technical difficulties make combining the 2 modalities challenging. It requires a careful design of both modalities to achieve performance and specifications similar to their stand-alone imaging counterparts. The main challenge is that the modalities interfere with each other; additionally, there are constraints on the space available for the components and absolute PET quantification has been challenging in PET/MR, mainly because correct attenuation maps are difficult to obtain with MR. Bone, metallic implants, MR hardware, and other dense materials significantly attenuate radiation but are difficult, if not impossible, to see on MR images.

Most of the challenges complicating PET/MR have, at least partially, been solved. In this review, we discuss the principles of combined PET/MR, the variety of available designs, recent and current detector technologies, and several PET/MR–specific

Received Mar. 21, 2014; revision accepted Apr. 24, 2014.
For correspondence or reprints contact: Bernd J. Pichler, Röntgenweg 13, 72076 Tübingen, Germany.
E-mail: bernd.pichler@med.uni-tuebingen.de
Published online May 12, 2014.

TABLE 1
Abbreviated* Overview of PET/MR Systems Described in Literature

Company or university	Year (ref)	Usage†	MR field strength (T)	Scintillator, detector‡	Crystal rings	Blocks/ ring	Crystal block (size [mm³])	Axial, transaxial FOV (cm)
University of California, Los Angeles, CA (US)	1997 (*6*)	P-R-Sim	0.2	LSO MC PMT + fibers	1	48	16§ (2×2×10)	1.0 <3.8
University of California, Los Angeles, CA (US)	1997 (*7*)	P-R-Sim	0.2 and 9.4	LSO MC PMT + fibers	1	72	24§ (2×2×5)	0.2 <5.4
Kings College, London (UK)	2005 (*80*)	P-R-Sim	3	LSO PS PMT + fibers	1	8	1×4×4 (2×3×5)	0.3 5.6
University of Cambridge, Cambridge (UK)	2006 (*28*)	P-R-Sim	1 (split magnet)	LSO PS PMT+ fibers	48	24	12×12 (1.52×1.52×10)	7.2 <14.7
West Virginia University, Morgantown, WV (US)	2007 (*81*)	P-R-Sim	3	LSO PS PMT + fibers	20	2	20×20 (2.5×2.5×15)	5.0 8.0
Kobe City College of Technology, Kobe (JP)	2009 (*25*)	P-R-Sim	0.15	MLS PS PMT + fibers	3	32	2×2×2 (2.5×3.5×3.5)	0.5 NA
Western Ontario, London, ON (CA)	2009 (*29*)	P-R-Seq	0.3 (field-cycled)	BGO PS PMT + fibers	8	2	8×8 (6.2×5.6×30)	~5.0 NA
Kobe City College of Technology, Kobe (JP)	2010 (*13*)	P-R-Sim	0.3	LGSO PS PMT + fibers	11	16	11×9×2 (1.9×2.2×6/7)	2.1 8.0
Nagoya University, Nagoya (JP)	2012 (*82*)	P-R-Sim	0.3	LGSO PS PMT + fibers	13	16	11×13×2 (0.9×1.3×5/6)	2.1 5.6
Mediso Ltd., Budapest (HU)	2013 (*12*)	P-Co-Seq	1	LYSO PS PMT	81	12	39×81 (1.12×1.12×13)	9.4 4.5-12.0
University of California, Davis, CA (US)	2006 (*15*)	P-R-Sim	7	LSO PS APD + fibers	8	16	8×8 (1.43×1.43×6)	1.2 3.5
University of Tübingen, Tübingen (DE)	2007 (*43*)	P-R-Sim	7	LSO APD	12	10	12×12 (1.6×1.6×4.5)	1.9 4.0
‖Brookhaven National Laboratory, Upton, NY (US)	2011 (*26*)	P-R-Sim	9.4	LSO APD	8	12	4×8 (2.2×2.2×5)	1.8 3.8
University of Tübingen, Tübingen (DE)	2013 (*42*)	P-R-Sim	7	LSO APD	45	16	15×15 (1.5×1.5×10)	7.2 7.2
Sogang University, Seoul (KR)	2011 (*83*)	P-R-Sim	3	LYSO SiPM	4	16	4×4 (3×3×10)	1.3 <7.0
Seoul National University, Seoul (KR)	2012 (*84*)	P-R-Sim	3	LGSO SiPM	20	12	20×18 (1.5×1.5×7)	3.2 13.6
RWTH Aachen, Aachen (DE)	2012 (*19*)	P-R-Sim	3	LYSO Digital SiPM	22	10	22×22 (1.3×1.3×10)	3.0 16.0
Eulji University, Gyeonggi (KR)	2012 (*85*)	P-R-Sim	3	LYSO SiPM + fibers	6	12	6×6 (2.47×2.74×20)	NA
Kobe City College of Technology, Kobe (JP)	2012 (*86*)	P-R-Sim	0.15	LGSO SiPM phoswich	11	16	11×9×2 (1.1×1.2×5/6)	13.2 8.0
Sogang University, Seoul (KR)	2013 (*87*)	P-R-Sim	3	LYSO SiPM	4	72	4×4 (3×3×20)	12.9 25.0
Koninklijke Philips NV, Eindhoven (NL)	2011 (*10*)	C-Co-Seq	3	PMT	44	28	23×44 (4×4×22)	18.0 60.0
Siemens AG, München (DE)	2008 (*8,27*)	C-R-Sim	3 and 9.4	APD	72	32	12×12 (2.5×2.5×20)	19.3 32.0
Siemens AG, München (DE)	2012 (*9*)	C-Co-Sim	3	APD	64	56	8×8 (4×4×20)	25.8 59.4
¶GE Healthcare, Waukesha, WI (US)	2014 (*11*)	C-Co-Sim	3	SiPM	45	112	4×9 (3.95×5.3×25)	25.0 60.0

*Full version of this table can be found as supplemental file at http://jnm.snmjournals.org.

†Code specifying field (P = preclinical; C = clinical), status (R = research; Co = commercial), and operation (Sim = simultaneous; Seq = sequential).

‡APD = avalanche photodiode; BGO = bismuth germanate; LGSO = lutetium gadolinium oxyorthosilicate; LSO = lutetium oxyorthosilicate; LYSO = lutetium yttrium oxyorthosilicate; MLS = mixed lutetium silicates; MC = multichannel; PMT = photomultiplier tube; PS = position-sensitive; SiPM = silicon photomultiplier.

§Describes number of crystals per MC-PMT.

‖A variant of this scanner has recently been introduced commercially by MR Solutions Ltd.

¶This scanner has been presented at Radiological Society of North America and Society of Nuclear Medicine and Molecular Imaging conferences but is not yet commercially available.

software approaches. Moreover, the foreseeable future of this recent hybrid technology is briefly discussed.

SYSTEM DESIGNS

Since the development of the first working prototype in 1997, various approaches have been taken to acquire PET and MR data with a single machine (*6,7*). There is a general distinction between systems that acquire images sequentially and those that can acquire images simultaneously, as well as between preclinical and clinical systems. Table 1 presents an overview of the systems reported in the literature, summarizing the different approaches and some of their major properties.

For systems that enable simultaneous data acquisition, there is a distinction between fully integrated systems and those with a PET insert that fits inside a standard MR scanner gantry. Sequential geometry is easier to implement because the 2 modalities can be placed at a distance that reduces mutual interference. However, simultaneous acquisition is a more promising approach given the much larger number of simultaneous systems presented in the literature. Simultaneously acquired images are intrinsically coregistered, both temporally and spatially, and the scanning time can be reduced with an integrated device.

The first hybrid PET/MR systems were designed for preclinical imaging, followed by clinical systems more than a decade later. One clinical PET/MR prototype was developed as an insert for brain imaging, and it used avalanche photodiode (APD) detectors (*8*) instead of the photomultiplier tubes (PMTs) traditionally used in PET. Two commercial PET/MR systems have since been introduced, and their overall designs are substantially different. One of these systems features simultaneous PET/MR acquisition, and it is based on a wide-gantry MR scanner with integrated APD PET detectors (*9*). The second scanner is a sequential system, which was built using 2 slightly modified standard scanners with a motorized bed in between (*10*). This scanner contains standard PMTs with additional shielding to detect the scintillation light. A third clinical system has recently been presented but has not been introduced commercially (*11*). The first commercially available combined system for preclinical research offers sequential imaging with PMT-based PET detectors, and the gantry is attached to a permanent 1-T MR magnet (*12*). In the following sections, the different technologies used in PET/MR are discussed in more detail.

PET

In hybrid PET/MR approaches, the 2 modalities can have mutual interference, degrading the image quality. The MR radiofrequency pulses or switching gradients can influence the PET electronics, and conversely, the PET components can distort the main magnetic field.

PET Detectors. Since the beginning of PET development, PMTs have been the devices of choice for detecting scintillation light. However, their strong sensitivity to magnetic fields hinders their use inside an MR scanner. Even the earth's magnetic field (~50 μT) affects PMTs, but low fields such as this can easily be shielded by covering the outside glass. However, the static magnetic field used in MR is several orders of magnitude stronger, making shielding a viable option only at a certain distance from the magnet. Figure 1 illustrates the effect of increasing field strengths on the operation of a PMT-based PET detector.

In some hybrid systems, only the scintillators have been placed inside the MR imager. The light is guided to PMTs through optical fibers; the PMTs have been placed outside the magnetic fringe field, at field strengths of less than 500 μT. Simultaneous imaging with this configuration is possible, but approximately 90% of the scintillation light is lost (*13*). With the loss of scintillation light, the energy resolution is drastically degraded.

To avoid the use of light fibers and their accompanying disadvantages, APDs have been used to replace PMTs because they are unaffected by magnetic fields. Their introduction has paved the way for new hybrid scanner designs that include photon detectors in the main MR magnetic field (*14*). In some instances, relatively short light fibers between scintillators and APDs have been used to move components that have a low magnetic permeability, such as front-end electronics, out of the FOV to reduce magnetic field disturbances (*15*). With the scintillator's low level of light energy flux and the low intrinsic amplification of APDs, a charge-sensitive preamplifier is required to convert the electron charge into a measureable voltage signal. The charge-sensitive preamplifier integrates the APD charge over several nanoseconds to achieve high conversion factors, with the disadvantage of pile-up events at high counting rates. The lower gain in APD-based systems requires more advanced front-end electronics. Therefore, most systems use an application-specific integrated circuit to help meet the electrical requirements, complexity, compactness, and performance. Because of the noise and the time variation in the electron drift during the avalanche multiplication process of APDs, the timing resolution is limited to approximately 1.8 ns in a block readout (*16*), which hinders the use of APDs in time-of-flight applications.

Approximately 10 y ago, the first Geiger-mode APD (G-APD) arrays were studied for low-light-level detection in high-energy physics. A single photon can trigger a self-sustaining ionization cascade, also called Geiger discharge, analogous to the operation of Geiger-Müller tubes. G-APD arrays feature a gain comparable to that for PMTs; they are therefore commonly known as silicon photomultipliers (SiPM). Other names include solid-state photomultipliers and multipixel photon counters.

The signal generated by a single G-APD does not carry any information about the energy or quantity of incoming particles. In PET scintillation detectors, γ-photon energy information is carried via the number of photons generated by the scintillator rather than by the photon wavelength or energy. To discern the amount of incident light, SiPMs consist of a grid of small G-APDs, or cells, at a level of 100 to 10,000 per mm^2. All individual cells are connected in parallel, and their signals are combined. The number of cells per surface area increases the dynamic range of the detector, and its output can provide information about the quantity of photons.

The main noise contribution in an SiPM output signal is from the so-called dark counts, which are signals generated by the detector itself. These signals are partly due to the optical crosstalk between cells, but they are mainly thermally generated. The dark counts increase by a factor of approximately 2 every 8°C (*17*). Also, the SiPM gain is strongly affected by the temperature (*18*). This is especially relevant for its application in an MR scanner because rapid gradient switching, the application of radiofrequency pulses, and the confined environment can induce large temperature variations. Therefore, temperature control is of particular importance for SiPM detectors in PET/MR.

Because of the high gain and fast response times of SiPMs, front-end electronics can be straightforward and do not necessarily require charge-sensitive preamplifiers and application-specific integrated circuits. Wehner et al. (*19*) recently showed an insert

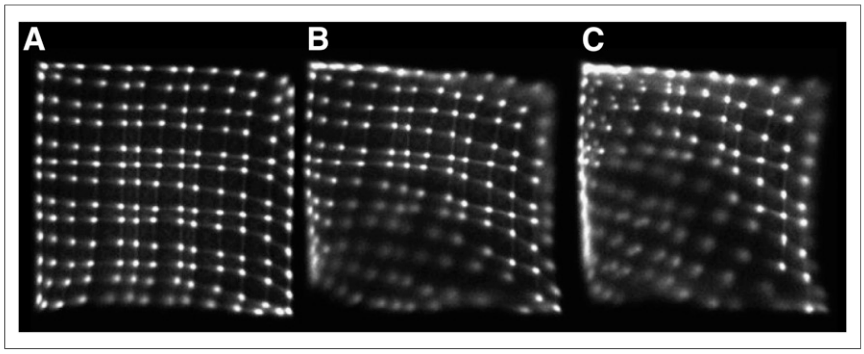

FIGURE 1. Effect of increasing magnetic field strength on crystal maps of PMT-based PET detector at 1 mT (A), 3 mT (B), and 5 mT (C). (Reprinted with permission of (*79*).)

based on SiPM technology with fully front-end digitizers. The signals from PET detectors are directly digitized and processed within the magnetic field. The single-photon detection capability of G-APDs enables triggering on the first photo electron, allowing for coincidence timing resolutions of 100 ps full width at half maximum or lower (*20*). Placement of SiPMs in strong magnetic fields has no effect on the energy and time resolutions (*21*). Because of their favorable properties, SiPMs are likely to replace PMTs, in PET/CT scanners as well, as demonstrated by a system recently introduced by Philips featuring digital SiPMs. More details about the 3 types of PET detectors have been listed by Lecomte (*22*).

Shielding. PET detector systems require sensitive preamplifiers and front-end electronics, which are also highly sensitive to electromagnetic interferences, such as the radiofrequency pulses generated by MR. To prevent MR sequences or gradient switching from degrading the PET signal quality or from generating false events, the electronic components should be placed at a distance or should be shielded (*23*). The integration of a PET system in an MR scanner requires a careful design of the radiofrequency shielding to avoid introducing eddy currents. These currents are introduced in conductors by changing magnetic fields, for example, applied gradients. Eddy currents create an additional magnetic field that can induce local magnetic field inhomogeneities as well as affect the gradient speed (slew rate) and the spatial encoding ability of the system (*23*). Furthermore, the PET components should consist of materials with a low magnetic susceptibility. Most integrated circuits fulfill this requirement, but components such as resistors, inductors, capacitors, or connectors should be equipped with nonmagnetic terminals to reduce artifacts.

Most PET systems do not cover the object or patient entirely; as a result, some of the radioactivity remains outside the FOV. Naturally, events caused by this radiation cannot be resolved because no coincidences will be detected. However, this radiation will increase the rate of scattered and random events. γ-ray shielding can be used to reduce this effect, but there are specific limitations on the materials used inside an MR scanner (*24*). Shielding materials should clearly be of high density to sufficiently attenuate γ photons, but shielding should have low conductivity to prevent the induction of eddy currents and to avoid influencing the radiofrequency signals. Moreover, the material should have a low magnetic susceptibility to guarantee a homogeneous magnetic field. Materials that fulfill these characteristics are lead and tungsten powders in combination with epoxy to reduce the conductivity (*24*).

MR

Significant modifications have to be made to the PET hardware to permit the acquisition of images in the presence of a strong magnetic field and radiofrequency pulses. In contrast, changes in the MR hardware are less obvious. Many of the various PET/MR prototype systems consist of a PET scanner that fits within the bore of a standard, unmodified MR scanner. Nevertheless, modifications to some of the MR components may improve the acquisition by reducing crosstalk between the 2 modalities and improving image quality.

Magnet. PET images have been acquired at different magnetic field strengths, from the 0.15-T permanent magnet setup used by Yamamoto et al. (*25*) to the 9.4-T systems for preclinical (*26*) and clinical applications (*27*). Hybrid systems usually consist of a commercially available stand-alone MR scanner combined with a custom built PET system. A notable exception was built with an only slightly modified, commercially available PMT-based PET system, but it features a 1-T split-magnet specifically designed for combined PET/MR (*28*). Another noteworthy example operates a PET scanner in a field-cycled MR system (*29*). During PET acquisition, the magnet is ramped down to enable normal operation of the PMT-based PET detectors.

The additional components required for PET acquisition result in a reduction in the bore size in hybrid systems. For example, the Siemens mMR system is based on a 70-cm, wide-bore MR scanner; however, the installed PET hardware reduces the bore diameter to 60 cm (*9*). In addition, the added components may distort the main magnetic field in simultaneous systems. A distorted magnetic field can decrease the MR image quality, especially for sequences that particularly rely on field uniformity, such as MR spectroscopy and echo planar imaging. However, several studies have shown that with sufficient shimming, the presence of additional PET hardware does not significantly affect the magnetic field homogeneity (*8,9,30*).

Gradient and Radiofrequency Coils. The gradient system is an essential component of an MR system. In the integrated or insert-based PET/MR scanners that have been described thus far, the PET detectors, electronics, and shielding reside within the gradient coils. This design can reduce the effectiveness of the gradients, decreasing the signal-to-noise ratio in the MR images (*14*). Rapid switching of the gradient coils, particularly evident in sequences such as echo planar imaging, produces resistive heat when the coils are energized (*31*). The heat can cause additional warming of the PET components. Because the operation of PET detectors, such as SiPMs, is strongly temperature-dependent, strict temperature control is required. Thus far, proposed hybrid systems have not used gradient coils specifically designed for combined PET/MR, with the exception of a gradient system for the split magnet proposed by Poole et al. (*32*). The gradient system and the magnet are split into 2 parts to house the PET detectors.

An integrated radiofrequency body coil can be used for whole-body imaging in MR scanners. However, because only weak radiofrequency signals emanate from the tissues during MR acquisition, and this particular coil is positioned relatively far away, this setup results in a low signal-to-noise ratio. Higher signal-to-noise ratios in MR images can be achieved with radio-

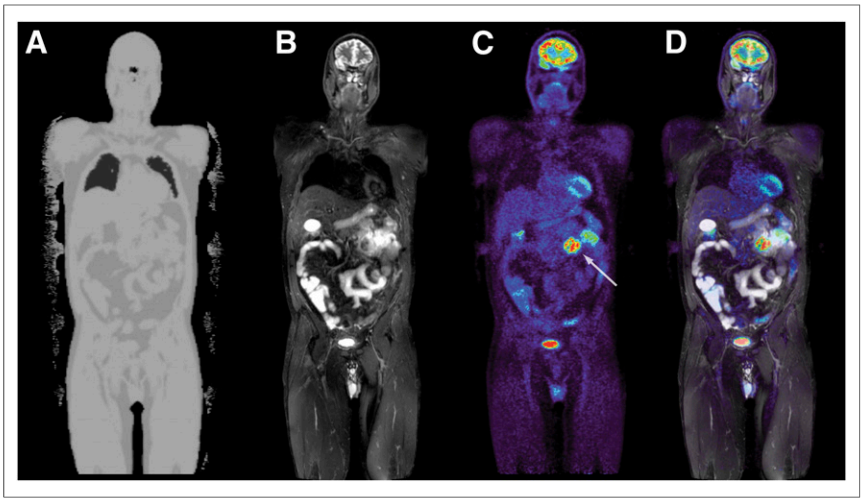

FIGURE 2. PET/MR image of patient with enteric melanoma metastasis (arrow): MR-based attenuation map (A), T2-weighted short-τ inversion recovery sequence (B), ^{18}F-FDG PET image (C), and PET overlaid on short-τ inversion recovery image (D). Data were acquired on a Biograph mMR system.

frequency receiver coils that are placed closer to the object of interest.

All coils placed in the FOV significantly attenuate radiation. It is worthwhile to optimize the coil design in PET/MR to reduce the attenuation losses. Still, even optimized coils attenuate and scatter radiation to some extent. For accurate quantification, attenuation maps of the coil elements in the FOV should be estimated and used during reconstruction. Because of a loss in counts, the global activity concentration will be underestimated when the coil is not accounted for in the attenuation correction (AC), but errors will be especially prevalent near the coil (*33–35*). The problem with the coils and other objects in the FOV, such as the bed, is that they provide no MR signal although they attenuate radiation. Coils with a fixed position can easily be measured beforehand, for example, with CT, and used as a template in the AC (*34,36*). In a similar manner, the bed can be included in the AC. However, coil placement should be fairly accurate because small misalignments could already create image artifacts and incorrect quantification (*33,36*). Additionally, the CT scan of the coils may have artifacts due to the metal components, which in turn can affect the PET images (*34*). An even more difficult challenge is attenuation due to flexible coils that can be placed in variable positions and orientations. In most cases, these coils are not included in the AC, but not including them could introduce significant deviations in the activity concentration. Attempts have been made to identify the coils using ultrashort echo time sequences or markers attached to the coil that are visible by both MR and CT (*37*).

Specially designed, low-attenuation coils in combination with accurate localization techniques can improve quantification of PET images. The standard coils available for MR have never been designed specifically for PET/MR; instead, they have been designed for optimal signal-to-noise ratio. PET/MR coils should have low attenuation for γ photons while still performing adequately. The optimization of radiofrequency coils for use in PET/MR is still a relatively young field, but initial studies show promising results (*38*). The homogeneity of the radiofrequency field could be influenced by the additional PET components, affecting the flip angle. Only very small radiofrequency field map differences have been reported in preclinical (*30*) and clinical (*8*) insert-based PET/MR systems.

CORRECTION METHODS AND RECONSTRUCTION

Standard MR protocols can be used for hybrid scanner acquisition, possibly supplemented with additional sequences for attenuation or motion correction. Standard clinical MR protocols can already require long acquisition times, especially when functional images are also acquired. In sequential scanners, PET and sequences for AC prolong the total acquisition, which could lead to unacceptably long acquisition times. Moreover, because of the time delay between MR and PET acquisition, differences in, for example, bladder filling between the 2 scans can lead to misregistrations (*39*). In simultaneous systems, images are more accurately registered (*40*) and the total acquisition times can be shorter because the anatomic images, AC sequences, and additional functional imaging can be acquired during the PET acquisition (*41*). However, misregistrations can occur because of the spatial deformation inherent to certain MR sequences (*40*).

Clinical considerations in PET/MR acquisition protocols are discussed for the Biograph mMR (Siemens) by Martinez-Möller et al. (*41*) and for the Ingenuity (Philips) by Vargas et al. (*39*). In preclinical imaging, both PET and MR images are usually acquired in 1 bed position (*42,43*).

AC

For quantitative PET imaging, the reconstructed data need to be corrected for the γ-photon attenuation. Direct measurement of linear attenuation coefficients is not possible in integrated PET/MR systems, and the problem needs to be addressed differently. MR information has to be converted to linear attenuation coefficients; however, because the MR signal relates to the proton density instead of to the γ-photon attenuation, this conversion is challenging. The available methods for MR-based AC can be grouped into the following 3 categories: segmentation-based methods, which segment the MR data into tissue classes and assign uniform linear attenuation coefficients to each tissue class; methods that use coregistered MR images and corresponding attenuation maps; and methods that use PET emission data and MR anatomic information to create attenuation maps. The AC possibilities depend on the subject of study, and the requirements differ between clinical and preclinical imaging.

Clinical Imaging. In brain imaging, the cranial bone significantly contributes to attenuation of the radioactivity in the brain because most lines of response intersect with the bone. Therefore, MR-based AC methods designed for brain imaging need to account for bone attenuation (*44,45*). However, it is not possible to delineate bone tissue solely from the intensity of single voxels with standard MR sequences because of its short T2 relaxation times.

With ultrashort echo time sequences, signal can still be acquired from bone and used to create attenuation maps. Proposed methods segment ultrashort echo time brain data into 3 (*46*) or 4 (*45*) tissue

classes, including bone tissue. Using such methods, a high correlation with the reference PET data using CT-based AC can be achieved, but regions with fine structure such as nasal cavities and cerebrospinal fluid are occasionally misclassified. AC methods for whole-body imaging need to address several challenges. Bone detection with MR is difficult because the current ultrashort echo time sequences are too time consuming to be applied for whole-body acquisitions in the clinical setting. However, unlike for brain imaging, whole-body applications are less affected when bone tissue is not properly discriminated from soft tissue in attenuation maps. Therefore, multiple groups have developed segmentation-based methods for whole-body MR-based AC that do not account for the bone without compromising the quantification accuracy for regions that are not close to osseous tissue. Lung segmentation needs to be addressed because the lung density between patients is highly variable, which can affect the quantification results (*47*). However, the lung signal intensity is generally low in images acquired with conventional MR sequences.

Martinez-Möller et al. (*48*) proposed a segmentation-based method that discriminates between air, lungs, fat, and soft tissue with intensity-based segmentation using fixed thresholds and connected component analysis to detect the lungs. The AC for the Biograph mMR system is based on this method. Figure 2 shows an attenuation map that was created on this system and the corresponding PET image for an example patient. Approaches that perform segmentation of 3 classes without distinguishing between fat and nonfat soft tissues have also been developed. The AC for the Ingenuity TF PET/MR system is based on such a method (*49*).

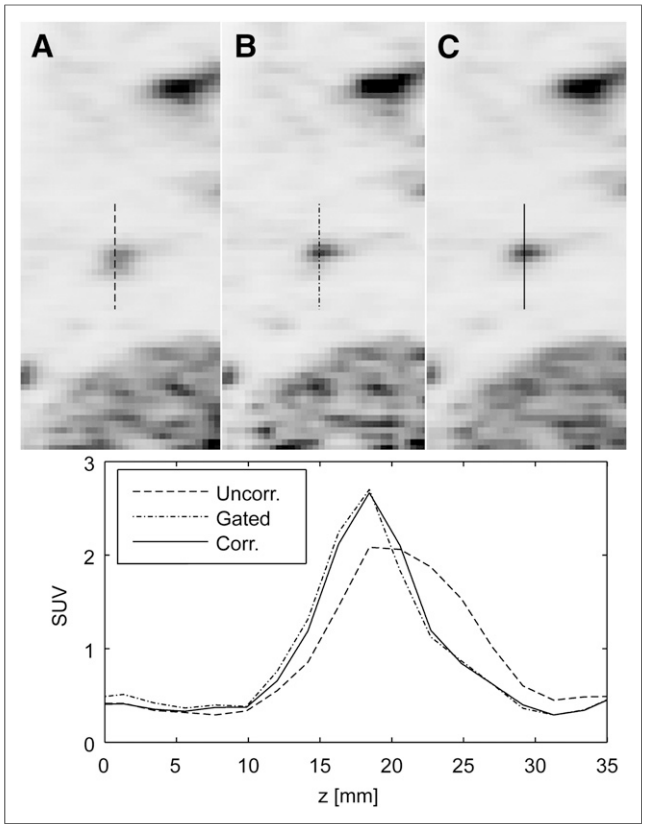

FIGURE 3. PET images and profiles through lung lesion: uncorrected (A), gated (B), and motion-corrected (C). (Reprinted with permission of (*64*).)

Atlas-based methods predict bone tissue without requiring specialized MR sequences. The attenuation maps can be created by deforming a single template image to match the patient anatomy (*50*) or averaging multiple coregistered attenuation template datasets (*51*). These methods can work well in brain imaging, but regions with high anatomic variability, such as the sinuses, prove to be challenging. Machine learning-based approaches offer another way to account for bone attenuation by learning a mapping from the MR to either the linear attenuation coefficient or CT data (*44*).

Atlas approaches or machine learning methods are more challenging for whole-body imaging than for brain imaging because of the high anatomic variability between patients and differences in the body position. Although segmentation-based methods that do not account for bone generally provide accurate quantification results for soft-tissue lesions (*52*), such methods can be complemented with bone prediction using an atlas or machine learning–based method.

Finally, the transaxial FOV of MR scanners is smaller than the patient cross section, which can lead to truncation artifacts in the MR images at the arm areas. These artifacts propagate to the attenuation maps created from the MR data if they are not adequately corrected. The truncation artifacts can be corrected using reconstructed PET images to derive the body outline (*53*) or by applying alternate emission and attenuation reconstruction techniques to estimate the missing parts of the attenuation map (*54*). Blumhagen et al. (*55*) proposed a method for extending the FOV via homogenization gradient enhancement, which might be an alternative to truncation artifact reduction without resorting to the PET data. Watson (*56*) proposed an approach for correcting truncation artifacts using supplemental transmission line sources placed around the periphery, whereas Mollet et al. (*57*) obtained a full attenuation map using an external radiation source. In addition to truncation artifacts, attenuation maps created from MR data can be affected by susceptibility artifacts in MR images. Metallic objects can cause nearby large image distortions or signal loss and affect the attenuation maps. Other intensity variations in MR images can also cause tissue misclassification, whereby, for example, the lungs may be falsely classified as air (*58*). A review of various MR-based AC techniques was given by Bezrukov et al. (*59*).

Preclinical Imaging. PET systems for preclinical small-animal imaging have less stringent attenuation map requirements due to the smaller subject size and shorter lines of response. An evaluation by Konik et al. (*60*) suggested that a uniform attenuation map computed by segmenting uncorrected PET data could provide sufficient accuracy below 6% for subjects smaller than 4 cm in diameter. Deriving attenuation maps from MR data is potentially more robust than segmenting uncorrected PET data, especially if highly specific tracers, such as ^{11}C-raclopride, are used. In studies with larger animals, additional tissue classes can be considered.

Motion Correction

Motion artifacts can significantly degrade the effective resolution of PET systems (*2*). A distinction between rigid motion (i.e., only rotation and translation), such as head movements, and nonrigid motion (i.e., changes in shape) can be made. Although patient motion can be reduced through patient cooperation or the use of positioning aids, nonrigid cardiac and respiratory motion needs to be accounted for with gating techniques or motion correction approaches.

In gating, list-mode data are filtered on the basis of the respiratory state or cardiac phase such that only counts from a single cardiac or respiratory state are used for image reconstruction. Because a large fraction of the acquired counts is discarded, the signal-to-noise ratio of the resulting images decreases unless the acquisition time is also prolonged. To prevent this decrease, techniques that keep the counts for all states by transforming them to a reference gating state have been developed. The transformation can be performed after the reconstruction, such that the images of different gating states are deformed to a reference state and summed (*61*), as well as during (*62*) or before the reconstruction (*63,64*).

The required deformation fields for performing the transformation can be obtained directly from the PET data by coregistering the individual reconstructed gating states. However, this approach is limited by the availability of the PET anatomic information. In simultaneous PET/MR systems, the deformation fields can instead be derived from MR data. For respiratory gating, the respiration signal can be extracted from navigator images (*64*), obviating an additional measurement device. Cardiac gating has been applied to PET/MR data using a trigger signal based on electrocardiography (*65*). Self-gated cardiac imaging has been developed for MR (*66*), but this method has yet to be applied for simultaneous PET/MR.

Several groups have proposed and evaluated methods for generating motion correction information from MR data using tagged MR sequences (*2*), embedded cloverleaf navigator–derived motion estimates (*63*), and 2-dimensional gradient echo images (*64*), with an example displayed in Figure 3.

MR-Guided PET Reconstruction

Because of the limited spatial resolution, PET images suffer from the partial-volume effect, which degrades their quantitative accuracy. Many approaches have been described to correct for the partial-volume effect, including deconvolution (*67*) and methods using the recovery coefficient of small objects (*68*). With hybrid PET/MR, the available anatomic information can be used for partial-volume correction. Some of these methods are applied after reconstruction (*69,70*), whereas other methods are integrated into the reconstruction process using anatomic images as prior information (*71*) or use wavelets (*72*). Reconstruction algorithms that incorporate MR-based anatomic information promote the formation of edges in the PET image at the transition between different tissue types. Recent approaches calculate the mutual information between PET and anatomic images to guide the reconstruction process and do not require prior segmentation of the anatomic images (*73*). Methods that use anatomic information in the PET reconstruction require good registration of the 2 imaging modalities. This registration is most easily achieved in the brain, and most of the proposed methods have therefore been applied only to brain imaging. Bai et al. (*3*) recently wrote an overview of MR–driven PET reconstruction.

DATA ANALYSIS

Although hybrid PET/MR scanners are commercially available, a significant proportion of PET/MR research has been performed on separate scanners, requiring registration of the images after acquisition. The registration quality depends on the region of interest; for example, the brain is relatively easy in that it requires only linear transformations, whereas whole-body imaging may be much more challenging. However, good results can be obtained when the subject does not have to be repositioned between scans, as has been shown in patients (*74*) and animals (*75*).

For a long time, it has been clear that MR information can facilitate defining PET regions of interest, thus facilitating PET image analysis (*76*). Atlases that map specific regions in the brain can be generated, and these can be registered to individual patients or animals. The high-resolution, high-contrast images acquired with MR are well suited for atlas registration, after which the PET images can be analyzed. With predefined regions of interest, brain function analysis can be performed in a more automated fashion, making the results less operator-dependent, more reproducible, and easier to compare with other studies. For image analysis of organs and tissues other than the brain, these approaches are not feasible because of the anatomic variations (including pathologies) between individuals and different positioning between scans. However, MR provides higher soft-tissue contrast than CT, making it easier to define regions of interest.

Apart from the anatomic information, which is useful for defining regions of interest, functional information can be obtained with MR. Although the sensitivity of MR is a few orders of magnitude lower than that of PET, substantial functional information can be collected simultaneously or in quick succession with PET. Both PET and MR provide information on equivalent or similar physiologic parameters, but the 2 modalities complement each other. Discrepancies can still be seen in direct comparisons, for example, between MR spectroscopy of endogenous choline and ^{11}C-choline PET (*77*).

The signal intensity in MR images has no absolute quantitative value but depends on many factors. Some of these, such as the T1 and T2 relaxation times and proton density, are tissue-related, but many others, such as the echo and repetition times and sensitivity of the coil, are not. However, quantification of MR is emerging; quantitative parameters such as the apparent diffusion coefficient and T1 or T2 relaxometry are being used not only in research but also in daily clinical practice (*78*). Advances in MR quantification will also be beneficial for hybrid PET/MR and may complement standard anatomic sequences.

The drawbacks of acquiring functional imaging data are the increased duration of studies and the large datasets that are obtained. It may become difficult to evaluate and use the data to their full potential. There is a clear role for machine learning approaches and medical informatics to improve analysis of PET/MR datasets. Techniques such as clustering could be used to identify or quantify irregularities in multimodal, multiparametric imaging data.

Combining PET with MR offers new opportunities for studying disease processes and biologic functions. Other imaging modalities may contribute additional information, but they too require image registration.

CONCLUSION

After more than a decade of continuous development, focusing mainly on new PET detector technology and the hardware integration of a PET scanner into an MR system, PET/MR has recently rapidly emerged from the first prototype systems into Food and Drug Administration–approved clinical scanners. Although there have been many technical challenges, PET/MR has matured to a reliable technology that can provide quantitative PET data, full MR functional imaging capabilities, and high-resolution anatomic MR images with superb soft-tissue contrast. The transition from research prototypes into clinical scanners, which provide all imaging options and perform the same as stand-alone systems, was rapid, given that a completely new generation of PET detec-

tors able to operate in high magnetic fields had to be developed. Interestingly, these novel and compact semiconductor G-APD light detectors will likely replace the conventional PMTs used in PET/CT systems. Therefore, the development of PET/MR technology might have initiated a new generation of PET scanners.

In addition to the changes in hardware, which are based on new concepts, there have been new developments in the image correction methods, such as MR-based attenuation or motion correction. Retrieving attenuation coefficients from the MR information might also be beneficial for future radiation therapy–planning projects that are based on MR images.

The development of PET/MR has triggered a shift in the PET detector technology and image correction paradigms. Most of the technical challenges have been solved, but clinical studies have yet to show the areas of patient care for which PET/MR is advantageous over other diagnostic methods.

DISCLOSURE

No potential conflict of interest relevant to this article was reported.

REFERENCES

1. Beyer T, Townsend DW, Brun T, et al. A combined PET/CT scanner for clinical oncology. *J Nucl Med.* 2000;41:1369–1379.
2. Ouyang J, Li Q, El Fakhri G. Magnetic resonance-based motion correction for positron emission tomography imaging. *Semin Nucl Med.* 2013;43:60–67.
3. Bai B, Li Q, Leahy RM. Magnetic resonance-guided positron emission tomography image reconstruction. *Semin Nucl Med.* 2013;43:30–44.
4. Hammer BE, Christensen NL, Heil BG. Use of a magnetic field to increase the spatial resolution of positron emission tomography. *Med Phys.* 1994;21:1917–1920.
5. Pelizzari CA, Chen GT, Spelbring DR, Weichselbaum RR, Chen CT. Accurate three-dimensional registration of CT, PET, and/or MR images of the brain. *J Comput Assist Tomogr.* 1989;13:20–26.
6. Shao Y, Cherry SR, Farahani K, et al. Simultaneous PET and MR imaging. *Phys Med Biol.* 1997;42:1965–1970.
7. Shao Y, Cherry SR, Farahani K, et al. Development of a PET detector system compatible with MRI/NMR systems. *IEEE Trans Nucl Sci.* 1997;44:1167–1171.
8. Kolb A, Wehrl HF, Hofmann M, et al. Technical performance evaluation of a human brain PET/MRI system. *Eur Radiol.* 2012;22:1776–1788.
9. Delso G, Fürst S, Jakoby B, et al. Performance measurements of the Siemens mMR integrated whole-body PET/MR scanner. *J Nucl Med.* 2011;52:1914–1922.
10. Zaidi H, Ojha N, Morich M, et al. Design and performance evaluation of a whole-body Ingenuity TF PET-MRI system. *Phys Med Biol.* 2011;56:3091–3106.
11. Levin C, Glover G, Deller T, McDaniel D, Peterson W, Maramraju SH. Prototype time-of-flight PET ring integrated with a 3T MRI system for simultaneous whole-body PET/MR imaging [abstract]. *J Nucl Med.* 2013;54(suppl 2):45P.
12. Nagy K, Tóth M, Major P, et al. Performance evaluation of the small-animal nanoScan PET/MRI system. *J Nucl Med.* 2013;54:1825–1832.
13. Yamamoto S, Imaizumi M, Kanai Y, et al. Design and performance from an integrated PET/MRI system for small animals. *Ann Nucl Med.* 2010;24:89–98.
14. Pichler BJ, Judenhofer MS, Catana C, et al. Performance test of an LSO-APD detector in a 7-T MRI scanner for simultaneous PET/MRI. *J Nucl Med.* 2006; 47:639–647.
15. Wu Y, Catana C, Farrell R, et al. PET performance evaluation of an MR-compatible PET insert. *IEEE Trans Nucl Sci.* 2009;56:574–580.
16. Grazioso R, Zhang N, Corbeil J, et al. APD-based PET detector for simultaneous PET/MR imaging. *Nucl Instrum Meth A.* 2006;569:301–305.
17. Renker D, Lorenz E. Advances in solid state photon detectors. *J Instrum.* 2009;4: P04004.
18. Kolb A, Lorenz E, Judenhofer MS, Renker D, Lankes K, Pichler BJ. Evaluation of Geiger-mode APDs for PET block detector designs. *Phys Med Biol.* 2010;55: 1815–1832.
19. Wehner J, Weissler B, Dueppenbecker P, et al. PET/MRI insert using digital SiPMs: investigation of MR-compatibility. *Nucl Instrum Meth A.* 2014;734: 116–121.
20. Schaart DR, Seifert S, Vinke R, et al. $LaBr_3$:Ce and SiPMs for time-of-flight PET: achieving 100 ps coincidence resolving time. *Phys Med Biol.* 2010;55:N179–189.
21. Spanoudaki VC, Mann AB, Otte AN, et al. Use of single photon counting detector arrays in combined PET/MR: characterization of LYSO-SiPM detector modules and comparison with a LSO-APD detector. *J Instrum.* 2007;2:12002–P12002.
22. Lecomte R. Novel detector technology for clinical PET. *Eur J Nucl Med Mol Imaging.* 2009;36(suppl 1):S69–S85.
23. Peng BJ, Walton JH, Cherry SR, Willig-Onwuachi J. Studies of the interactions of an MRI system with the shielding in a combined PET/MRI scanner. *Phys Med Biol.* 2010;55:265–280.
24. Strul D, Cash D, Keevil SF, Halsted P, Williams SCR, Marsden PK. Gamma shielding materials for MR-compatible PET. *IEEE Trans Nucl Sci.* 2003;50:60–69.
25. Yamamoto S, Hatazawa J, Imaizumi M, et al. A multi-slice dual layer MR-compatible animal PET system. *IEEE Trans Nucl Sci.* 2009;56:2706–2713.
26. Maramraju SH, Smith SD, Junnarkar SS, et al. Small animal simultaneous PET/MRI: initial experiences in a 9.4 T microMRI. *Phys Med Biol.* 2011;56: 2459–2480.
27. Shah NJ, Oros-Peusquens A-M, Arrubla J, et al. Advances in multimodal neuroimaging: hybrid MR-PET and MR-PET-EEG at 3 T and 9.4 T. *J Magn Reson.* 2013;229:101–115.
28. Hawkes RC, Fryer TD, Siegel S, Ansorge RE, Carpenter TA. Preliminary evaluation of a combined microPET-MR system. *Technol Cancer Res Treat.* 2010;9: 53–60.
29. Bindseil GA, Gilbert KM, Scholl TJ, Handler WB, Chronik BA. First image from a combined positron emission tomography and field-cycled MRI system. *Magn Reson Med.* 2011;66:301–305.
30. Wehrl HF, Judenhofer MS, Thielscher A, Martirosian P, Schick F, Pichler BJ. Assessment of MR compatibility of a PET insert developed for simultaneous multiparametric PET/MR imaging on an animal system operating at 7 T. *Magn Reson Med.* 2011;65:269–279.
31. Chu KC, Rutt BK. MR gradient coil heat dissipation. *Magn Reson Med.* 1995;34: 125–132.
32. Poole M, Bowtell R, Green D, et al. Split gradient coils for simultaneous PET-MRI. *Magn Reson Med.* 2009;62:1106–1111.
33. Tellmann L, Quick HH, Bockisch A, Herzog H, Beyer T. The effect of MR surface coils on PET quantification in whole-body PET/MR: results from a pseudo-PET/MR phantom study. *Med Phys.* 2011;38:2795–2805.
34. Aklan B, Paulus DH, Wenkel E, et al. Toward simultaneous PET/MR breast imaging: systematic evaluation and integration of a radiofrequency breast coil. *Med Phys.* 2013;40:024301.
35. Wollenweber SD, Delso G, Deller T, Goldhaber D, Hüllner M, Veit-Haibach P. Characterization of the impact to PET quantification and image quality of an anterior array surface coil for PET/MR imaging. *MAGMA.* 2014;27:149–159.
36. Delso G, Martinez-Möller A, Bundschuh RA, et al. Evaluation of the attenuation properties of MR equipment for its use in a whole-body PET/MR scanner. *Phys Med Biol.* 2010;55:4361–4374.
37. Paulus DH, Braun H, Aklan B, Quick HH. Simultaneous PET/MR imaging: MR-based attenuation correction of local radiofrequency surface coils. *Med Phys.* 2012;39:4306–4315.
38. Sander CY, Cramer A, Keil B, Mareyam A, Rosen BR, Wald LL. Low 511keV-attenuation array coil setup for simultaneous PET/MR imaging of the monkey brain. Presented at: International Society for Magnetic Resonance in Medicine 21st Annual Meeting and Exhibition; April 20–26, 2013; Salt Lake City, Utah; 2013.
39. Vargas M-I, Becker M, Garibotto V, et al. Approaches for the optimization of MR protocols in clinical hybrid PET/MRI studies. *MAGMA.* 2013;26:57–69.
40. Rakheja R, DeMello L, Chandarana H, et al. Comparison of the accuracy of PET/CT and PET/MRI spatial registration of multiple metastatic lesions. *AJR.* 2013;201:1120–1123.
41. Martinez-Möller A, Eiber M, Nekolla SG, et al. Workflow and scan protocol considerations for integrated whole-body PET/MRI in oncology. *J Nucl Med.* 2012;53:1415–1426.
42. Wehrl HF, Hossain M, Lankes K, et al. Simultaneous PET-MRI reveals brain function in activated and resting state on metabolic, hemodynamic and multiple temporal scales. *Nat Med.* 2013;19:1184–1189.
43. Judenhofer MS, Wehrl HF, Newport DF, et al. Simultaneous PET-MRI: a new approach for functional and morphological imaging. *Nat Med.* 2008;14:459–465.
44. Hofmann M, Steinke F, Scheel V, et al. MRI-based attenuation correction for PET/MRI: a novel approach combining pattern recognition and atlas registration. *J Nucl Med.* 2008;49:1875–1883.
45. Berker Y, Franke J, Salomon A, et al. MRI-based attenuation correction for hybrid PET/MRI systems: a 4-class tissue segmentation technique using a combined ultrashort-echo-time/Dixon MRI sequence. *J Nucl Med.* 2012;53:796–804.

46. Keereman V, Fierens Y, Broux T, De Deene Y, Lonneux M, Vandenberghe S. MRI-based attenuation correction for PET/MRI using ultrashort echo time sequences. *J Nucl Med.* 2010;51:812–818.
47. Marshall HR, Prato FS, Deans L, Théberge J, Thompson RT, Stodilka RZ. Variable lung density consideration in attenuation correction of whole-body PET/MRI. *J Nucl Med.* 2012;53:977–984.
48. Martinez-Möller A, Souvatzoglou M, Delso G, et al. Tissue classification as a potential approach for attenuation correction in whole-body PET/MRI: evaluation with PET/CT data. *J Nucl Med.* 2009;50:520–526.
49. Hu Z, Ojha N, Renisch S, et al. MR-based attenuation correction for a whole-body sequential PET/MR system. *IEEE Nucl Sci Symp Conf Rec*. 2009: 3508–3512.
50. Schreibmann E, Nye JA, Schuster DM, Martin DR, Votaw J, Fox T. MR-based attenuation correction for hybrid PET-MR brain imaging systems using deformable image registration. *Med Phys.* 2010;37:2101–2109.
51. Malone IB, Ansorge RE, Williams GB, Nestor PJ, Carpenter TA, Fryer TD. Attenuation correction methods suitable for brain imaging with a PET/MRI scanner: a comparison of tissue atlas and template attenuation map approaches. *J Nucl Med.* 2011;52:1142–1149.
52. Bezrukov I, Schmidt H, Mantlik F, et al. MR-based attenuation correction methods for improved PET quantification in lesions within bone and susceptibility artifact regions. *J Nucl Med.* 2013;54:1768–1774.
53. Delso G, Martinez-Möller A, Bundschuh RA, Nekolla SG, Ziegler SI. The effect of limited MR field of view in MR/PET attenuation correction. *Med Phys.* 2010;37:2804–2812.
54. Nuyts J, Bal G, Kehren F, Fenchel M, Michel C, Watson C. Completion of a truncated attenuation image from the attenuated PET emission data. *IEEE Trans Med Imaging.* 2013;32:237–246.
55. Blumhagen JO, Ladebeck R, Fenchel M, Scheffler K. MR-based field-of-view extension in MR/PET: B0 homogenization using gradient enhancement (HUGE). *Magn Reson Med.* 2013;1057:1047–1057.
56. Watson CC. Supplemental transmission method for improved PET attenuation correction on an integrated MR/PET. *Nucl Instrum Meth A.* 2014;734:191–195.
57. Mollet P, Keereman V, Bini J, Izquierdo-Garcia D, Fayad ZA, Vandenberghe S. Improvement of attenuation correction in time-of-flight PET/MR imaging with a positron-emitting source. *J Nucl Med.* 2014;55:329–336.
58. Keller SH, Holm S, Hansen AE, et al. Image artifacts from MR-based attenuation correction in clinical, whole-body PET/MRI. *MAGMA.* 2013;26:173–181.
59. Bezrukov I, Mantlik F, Schmidt H, Schölkopf B, Pichler BJ. MR-based PET attenuation correction for PET/MR imaging. *Semin Nucl Med.* 2013;43:45–59.
60. Konik A, Koesters T, Madsen MT, Sunderland JJ. Evaluation of attenuation and scatter correction requirements as a function of object size in small animal PET imaging. *IEEE Trans Nucl Sci.* 2011;58:2308–2314.
61. Dikaios N, Izquierdo-Garcia D, Graves MJ, Mani V, Fayad ZA, Fryer TD. MRI-based motion correction of thoracic PET: initial comparison of acquisition protocols and correction strategies suitable for simultaneous PET/MRI systems. *Eur Radiol.* 2012;22:439–446.
62. Chun SY, Reese TG, Ouyang J, et al. MRI-based nonrigid motion correction in simultaneous PET/MRI. *J Nucl Med.* 2012;53:1284–1291.
63. Catana C, van der Kouwe A, Benner T, et al. Toward implementing an MRI-based PET attenuation-correction method for neurologic studies on the MR-PET brain prototype. *J Nucl Med.* 2010;51:1431–1438.
64. Würslin C, Schmidt H, Martirosian P, et al. Respiratory motion correction in oncologic PET using T1-weighted MR imaging on a simultaneous whole-body PET/MR system. *J Nucl Med.* 2013;54:464–471.
65. Büscher K, Judenhofer MS, Kuhlmann MT, et al. Isochronous assessment of cardiac metabolism and function in mice using hybrid PET/MRI. *J Nucl Med.* 2010;51:1277–1284.
66. Larson AC, White RD, Laub G, McVeigh ER, Li D, Simonetti OP. Self-gated cardiac cine MRI. *Magn Reson Med.* 2004;51:93–102.
67. Teo B-K, Seo Y, Bacharach SL, et al. Partial-volume correction in PET: validation of an iterative postreconstruction method with phantom and patient data. *J Nucl Med.* 2007;48:802–810.
68. Avril N, Bense S, Ziegler SI, et al. Breast imaging with fluorine-18-FDG PET: quantitative image analysis. *J Nucl Med.* 1997;38:1186–1191.
69. Müller-Gärtner HW, Links JM, Prince JL, et al. Measurement of radiotracer concentration in brain gray matter using positron emission tomography: MRI-based correction for partial volume effects. *J Cereb Blood Flow Metab.* 1992;12: 571–583.
70. Rousset OG, Ma Y, Evans AC. Correction for partial volume effects in PET: principle and validation. *J Nucl Med.* 1998;39:904–911.
71. Leahy R, Yan X. Incorporation of anatomical MR data for improved functional imaging with PET. In: Colchester ACF, Hawkes DJ, eds. *Information Processing in Medical Imaging, 12th International Conference*. New York, NY: Springer Verlag; 1991:105–120.
72. Boussion N, Hatt M, Lamare F, et al. A multiresolution image based approach for correction of partial volume effects in emission tomography. *Phys Med Biol.* 2006;51:1857–1876.
73. Tang J, Rahmim A. Bayesian PET image reconstruction incorporating anato-functional joint entropy. *Phys Med Biol.* 2009;54:7063–7075.
74. Veit-Haibach P, Kuhn FP, Wiesinger F, Delso G, von Schulthess GK. PET-MR imaging using a tri-modality PET/CT-MR system with a dedicated shuttle in clinical routine. *MAGMA.* 2013;26:25–35.
75. Schmid A, Schmitz J, Mannheim JG, et al. Feasibility of sequential PET/MRI using a state-of-the-art small animal PET and a 1 T benchtop MRI. *Mol Imaging Biol.* 2013;15:155–165.
76. Evans AC, Beil C, Marrett S, Thompson CJ, Hakim A. Anatomical-functional correlation using an adjustable MRI-based region of interest atlas with positron emission tomography. *J Cereb Blood Flow Metab.* 1988;8:513–530.
77. Wehrl HF, Schwab J, Hasenbach K, et al. Multimodal elucidation of choline metabolism in a murine glioma model using magnetic resonance spectroscopy and ^{11}C-choline positron emission tomography. *Cancer Res.* 2013;73:1470–1480.
78. Tofts PS, Gowland PA, Stevenson VL, et al. in: Tofts PS, ed. *Quantitative MRI of the Brain: Measuring Changes Caused by Disease.* Somerset, NJ: Wiley; 2003: 1–650.
79. Vaquero JJ, Sánchez JJ, Udías JM, Cal-González J, Desco M. MRI compatibility of position-sensitive photomultiplier depth-of-interaction PET detectors modules for in-line multimodality preclinical studies. *Nucl Instrum Meth A.* 2013;702: 83–87.
80. Mackewn JE, Halsted P, Charles-Edwards G, et al. Performance evaluation of an MRI-compatible pre-clinical PET system using long optical fibers. *IEEE Trans Nucl Sci.* 2010;57:1052–1062.
81. Raylman RR, Majewski S, Velan SS, et al. Simultaneous acquisition of magnetic resonance spectroscopy (MRS) data and positron emission tomography (PET) images with a prototype MR-compatible, small animal PET imager. *J Magn Reson.* 2007;186:305–310.
82. Yamamoto S, Watabe H, Kanai Y, et al. Development of a flexible optical fiber based high resolution integrated PET/MRI system. *Med Phys.* 2012;39:6660–6671.
83. Kang J, Choi Y, Hong KJ, et al. A small animal PET based on GAPDs and charge signal transmission approach for hybrid PET-MR imaging. *J Instrum.* 2011;6: P08012–P08012.
84. Yoon HS, Ko GB, Kwon SI, et al. Initial results of simultaneous PET/MRI experiments with an MRI-compatible silicon photomultiplier PET scanner. *J Nucl Med.* 2012;53:608–614.
85. Hong SJ, Kang HG, Ko GB, Song IC, Rhee J-T, Lee JS. SiPM-PET with a short optical fiber bundle for simultaneous PET-MR imaging. *Phys Med Biol.* 2012;57:3869–3883.
86. Yamamoto S, Watabe T, Watabe H, et al. Simultaneous imaging using Si-PM-based PET and MRI for development of an integrated PET/MRI system. *Phys Med Biol.* 2012;57:N1–N13.
87. Hong KJ, Choi Y, Jung JH, et al. A prototype MR insertable brain PET using tileable GAPD arrays. *Med Phys.* 2013;40:042503.

The Journal of NUCLEAR MEDICINE

Principles of PET/MR Imaging

Jonathan A. Disselhorst, Ilja Bezrukov, Armin Kolb, Christoph Parl and Bernd J. Pichler

J Nucl Med. 2014;55:2S-10S.
Published online: May 12, 2014.
Doi: 10.2967/jnumed.113.129098

The Journal of Nuclear Medicine is published monthly.
SNMMI | Society of Nuclear Medicine and Molecular Imaging
1850 Samuel Morse Drive, Reston, VA 20190.
(Print ISSN: 0161-5505, Online ISSN: 2159-662X)

SNMMI SOCIETY OF NUCLEAR MEDICINE AND MOLECULAR IMAGING